Solvation Effects, Reactivity Studies and Molecular Dynamics of Two Phosphonic Acids – Theoretical Investigation

Jamelah S. Al-Otaibi, Y. Sheena Mary, Y. Shyma Mary, Sreejit Soman & M. Thirunavukkarasu

View supplementary material ↗

Published online: 27 Sep 2022.

Submit your article to this journal ↗

Article views: 20

View related articles ↗

View Crossmark data ↗

Taylor & Francis
Taylor & Francis Group

Check for updates

Solvation Effects, Reactivity Studies and Molecular Dynamics of Two Phosphonic Acids – Theoretical Investigation

Jamelah S. Al-Otaibi[a], Y. Sheena Mary[b], Y. Shyma Mary[b], Sreejit Soman[c], and M. Thirunavukkarasu[d,e]

[a]Department of Chemistry, College of Science, Princess Nourah Bint Abdulrahman University, Riyadh, Saudi Arabia; [b]Thushara, Kollam, India; [c]Stemskills Research and Education Lab Private Limited, Faridabad, India; [d]Department of Physics, Indo-American College, Cheyyar, India; [e]Department of Physics, Thiru A Govindasamy Govt. Arts College, Tindivanam, India

ABSTRACT

Cancer metastasis or the spread of cancer cells from main tumor to other parts of the body is the most common cause of morbidity and mortality in cancer patients. Due to applications of risedronate (RES) and zoledronate (ZLA) in the medical field, the solvation effects, reactivity studies, and molecular dynamics (MD) are reported. The solvation-free energy in water (hydration-free energy) indicates good solubility in an aqueous medium, a factor that corroborates the biological activity. The O … H distances (P=O to OH) gives interactions in vacuum and solvents. Change in free energy for the RES and ZLA with both solvents indicated the process happen in spontaneously. Van der walls interactions demonstrated that the intramolecular hydrogen bonds at O4–C15 (RES) and at O8–H21, O3–H22, N10–H19, and O6–H17 (ZLA). MD and simulation of the ligand bound main WNT5A were studied in details to understand the nature of possible binding motifs and structurally stable conformations.

1. Introduction

Cancer metastasis or the spread of cancer cells is the leading issue among cancer patients. After the lung and liver, the bone is one of the most prevalent locations for metastatic metastasis.[1,2] Inadequate pain control in metastatic cancer patients is frequently accompanied with sadness, anxiety, diminished function, and a much lower quality of life, resulting in morbidity and death.[3] As a result in addition to the continued difficulty of discovering new treatments capable of curing the illness, there is a need to develop medications that provide palliative care to patients in order to relieve pain.

Diphosphonic acid has more coordination sites than monophosphonates, which has sparked major concern about the phosphate ligand. The bisphosphonic acid has three oxygen atoms on both ends, resulting in hexa-coordinated chemical ligands. Theoretically, both ends should be three coordinated, but the analysis demonstrates that both ends are two or one coordinated in some form.[4–7] Phosphonates give more bridging modes to metals than other organic compounds, making the production of structural motifs.[8] Nikfar and Shariatinia reported the DFT studies of phosphate functionalized carbon nanotubes as efficient drug delivery systems.[9] Biphosphonates

are natural pyrophosphate derivatives that are an important class of medications used to treat a variety of cancers.[10,11]

Risedronate (RES) is used to treat osteroporosis by effectively blocking bone resorption. Additionally, RES has been shown to have antiparasitic effects.[12,13] Zoledronate (ZLA) also known as zoledronic acid is a bisphosphonate medication that is administered intravenously to treat a variety of bone ailments. It also possesses anticancer properties and increases the efficiency of other antitumor chemicals when used together.[14] In postmenopausal women, ZLA enhanced bone density and reduced vertebral fractures.[15] Several organizations have looked into metal phosphate and phosphonate compounds as solid state materials for organizing organic molecules.[16] Mixed metal phosphonates can be made by combining phosphoric and phosphonic acids during the synthesis process.[16] Acids, bases, and anions and light emitting characteristics are obviously susceptible to imidazole based compounds.[17,18] Myller et al. reported pH behavior of a phosphate molecule.[19] Wnt5A signaling is critical for tumor genesis and skeletal remodeling. However, its role in the development of metastatic bone lesions is yet unknown. The complexity of Wnt5A signaling, which involves various ligands, receptors, and inhibitors, with intricate biological effects and unique signaling pathways depending on the cellular context, is one of the primary challenges in understanding its function in cancer progression.[20]

To predict and comprehend the features molecular systems, theoretical approaches to the study of the electronic structures are often used.[21] These computational tools are frequently employed in the study of organic molecules that could be used in pharmaceuticals.[22] Molecular modeling has developed into a very useful and effect tool in recent years. This method provides a strong alternative for the analysis of the experimental data. Without having to go through the experience, it enables the computerized investigation and therapy of chemical issues. A review of the literature reveals that modeling has established a very important place in the science of phosphonates compounds, as indicated by the research that are published on it every year.[23,24] The solvation-free energy calculates the energy changes in a molecule's transfer from gas to solvent and it is used to calculate a variety of properties like activity coefficients and solubilities. The solvation effects, reactivity studies, and molecular dynamics (MD) of (1-Hydroxy-1-phosphono-2-pyridin-3-ylethyl)phosphonic acid (RES) and (1-hydroxy-2-imidazol-1-yl-1-phosphonoethyl)phosphonic acid (ZLA) are reported due to its biomedical characteristics in this work.

2. Methods

Theoretical analysis of RES and ZLA (Figure 1) were done by Gaussian09 and GaussView5 at CAM-B3LYP-/6-311++G(d).[25,26] The default settings were used for the convergence criteria regarding SCF and optimization procedure. Topological features were examined for RES and ZLA
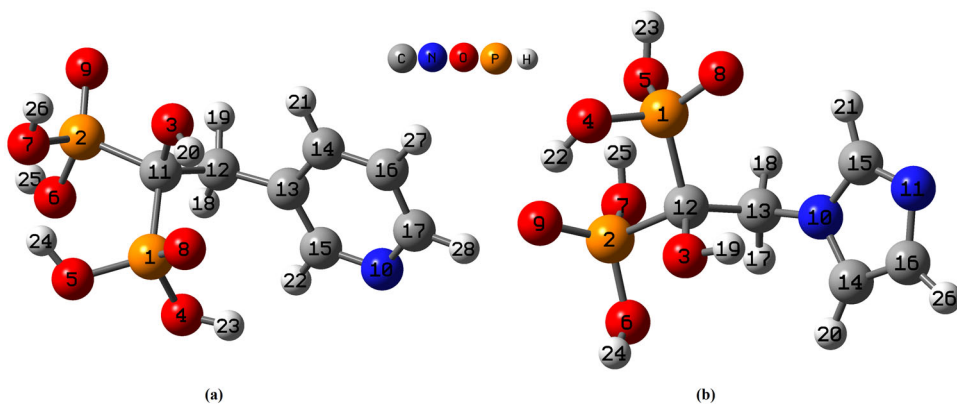

Figure 1. Optimized geometries of (a) RES and (b) ZLA.

by the AIM, RDG, ELF, and LOL, studies using Multiwfn program and AIMAll software.[27,28] In this study, due to absence of available X-ray crystallography structure of Wnt5A in the structural databases such as PDB and MMDB, the protein was homology modeled in deep mind's Alpha fold.[29] The primary sequence of Wnt5a was taken from Uniprot database (ID:UniProtKB- P41221 (WNT5A_HUMAN)) and modeled in Alpha fold version 2.0. Final energy-minimized model was validated by ProSa and PROCHECK for Ramachandran plot, 1 D-3D, and Errat plot analysis.[30,31] In order to study the molecular interactions of major pathway protein Wnt5A responsible for bone cancer and ligands, ZLA and RES, the structures were energy minimized with AMBER 14ff for atom type correction and Gasteiger charges were added. Docking was performed with Autodock.[32] During molecular docking studies, three replicates were performed. The total number of solutions was computed 50 in each case, with population size 500, number of evaluations 2,500,000, maximum number of generations 27,000, and rest the default parameters were allowed. After docking, the RMSD clustering maps were obtained by reclustering command with a clustering tolerance of 0.25, 0.5, and 1 Å, respectively, to get the best cluster with the lowest energy score with a high number of populations. The Ki values were determined from the free energy of binding energy using present algorithm in Autodock version 4.2.6.

The MD simulations studies were carried on the docked complexes for protein with ligand using the Desmond 2020.1 from Schrödinger, LLC. The sampling was done using same parameters for MD with OPLS-2005[33–35] and explicit model with SPC water molecules were used in this system.[36] MD simulations were performed on WNT5A for 100 ns. NaCl solutions (0.15 M) were added to simulate physiological environment. Initially, system was equilibrated using NVT ensemble for 100 ps to retain over the protein-ligand complex. Followed by this a short run equilibration and minimization using NPT ensemble for 12 ps and as reported.[37–39] To find the bonded forces for each trajectory RESPA integrator was used for a time step of 2 fs. The RMSD, Rg, RMSF, and H-bonds were calculated to study the stability of the MD simulations.

3. Results and discussion

3.1. Electronic and chemical properties

Solvation-free energies (SFE) in water and DMSO were obtained by Truhlar's SMD,[40] which uses set of parameters calculated along with IEF-PCM. SFE estimates energy change of the molecule in the environments, gaseous and solvent, being important for determine different properties.[41] The SFE were calculated *via* SMD model in water and DMSO are −29.61, −19.33 for RES and −26.85, −22.55 kcal/mol for ZLA. Although the values obtained be negative for all solvents tested, the comparison of SFE values suggests that water may be better for the solubilization of RES and ZLA. Value of SFE in water indicates good solubility in an aqueous medium, factor that corroborates the biological activity, in as much as that bioorganic processes occur in aqueous medium.

In addition, the thermochemical quantities and their changing were presented in Table S1. Accordingly, for RES, in water the changes are high while for ZLA the changes are nearly same. The changes of the entropy during the process for all water and DMSO with RES are negative while for ZLA with water the change is positive. Besides, the changing of the free energy (negative values of ΔG) for the RES and ZLA with both solvents indicated the solvation process happen in spontaneously. Whether a chemical change is thermodynamically feasible is dependent on Gibbs energy and its variations. As a result, the reaction will tend to occur spontaneously. However, if the free energy of the products is greater than that of the reactants, the reaction will not take the course indicated and will instead tend to go in the opposite direction.[42] Namely, the ΔG quantities of RES and ZLA were calculated as −29.59, −20.16 and −27.85, −23.11 kcal/mol, respectively. Also, the lowest ΔS quantities of the RES and ZLA with DMSO were calculated as −0.004 and −0.832 kcal/mol, respectively (Table S1).

Table 1. Chemical descriptors (eV).

	E_{HOMO}	E_{LUMO}	Energy gap	Hardness	Chemical potential	Electrophilicity index
RES						
Vacuum	−8.6849	−0.3962	8.2887	4.1444	−4.5406	2.4873
Water	−8.3736	−0.615	7.7521	3.8761	−4.4976	2.6093
DMSO	−8.4419	−0.5801	7.8618	3.9309	−4.5110	2.5884
ZLA						
Vacuum	−7.9271	−1.3260	6.6011	3.3006	−4.6266	3.2426
Water	−7.6822	−2.0501	5.6321	2.8161	−4.8662	4.2043
DMSO	−7.6719	−1.7516	5.9203	2.9602	−4.7118	3.7498

Ionization potential, $I = -E_{HOMO}$ and electron affinity, $A = -E_{LUMO}$. I, A, and energy gap are, 8.6849, 0.3962, 8.2887/8.9271, 1.3260, 6.6011 eV for RES/ZLA in vacuum (Table 1). The chemical descriptors of RES/ZLA in vacuum are: hardness, $\eta = 4.1444/3.3006$ eV, chemical potential, $\mu = -4.5406/-4.6266$ eV, and electrophilicity index, $\omega = 2.4873/3.2425$ eV, respectively.[43,44] Hardness values for phosphonate derivatives are reported to be between 3.13 and 3.32 eV, chemical potential values between −3.62 and −3.67 eV, and electrophilicity index in the range 2.00–2.09 eV.[45] Table 1 shows that theoretical FMOs energies and HOMO–LUMO gap calculated for RES/ZLA are somewhat lower in solution, indicating that dielectric constant changes reactivity of RES/ZLA, directly affecting the reactivity, revealing lower hardness and electrophilicity index in solvents. However, in general, the calculated global reactivity descriptors compared to calculated ones for other bioactive molecules in literature[46] indicates the studied molecule as a soft molecule with good attractive electron power and moderate donating electron power.

In vacuum, the UV–vis absorptions of RES are at 220.39 and 241.10 nm while, in solvents, only one absorption is seen nearly at 222 nm for water and DMSO (Figure S1). For ZLA, two absorptions are nearly at 172 and 186 nm in vacuum and solvents, with a slight lowering in water for the band 172 nm.

3.2. Spectroscopic properties

Most of the bond lengths are changing due to solvation of RES and ZLA (Table S2). The P-O bond lengths are changing by 0.0152–0.0010 Å (water), 0.0053–0.0002 Å (DMSO), C-P bond lengths by 0.0156–0.0077 Å (water), 0.0037–0.0022 Å (DMSO) for RES and 0.0528–0.0013 Å (water), 0.0191–0.0000 Å (DMSO), C–P lengths by 0.0095–0.0034 Å (water), 0.0092–0.0030 Å (DMSO) for ZLA. The H atoms of OH to O atom of P=O are at distances, 1.9237, 2.6606, 2.6563/2.5361, 2.8859, 2.7513/1.9861, 2.8039, 2.6863 Å (O8-H20, O9-H25, and O8-H23) for RES and 2.8534, 2.7149/2.8417, 2.9204/2.8621, 2.8059 Å (O9-H25, O8-H23) for ZLA in vacuum/water/DMSO, respectively, giving the hydrogen bond interactions in the systems.

In solvents maximum deviations are observed for the vibrational modes (Figure S2 and Table S3) at 3639, 3627, 3622, 3515, 1390, 620, 569, 521 cm^{-1} for RES and for ZLA, 3644, 3629, 3247, 1305, 1244, 1100, 1077 923, 449 cm^{-1} (vacuum; deviations of more than 20 cm^{-1}). Also in water a number of modes show deviations greater than that in DMSO and probably these shifts are due to hydrogen bonding in the systems. DFT gives υOH in the range 3639–3423 cm^{-1} for RES and at 3644–3247 cm^{-1} for ZLA.[47] The FTIR modes of PO$_4$ vibrations are reported in the ranges at 550–600 cm^{-1} (υ4), 961 cm^{-1} (υ1), 1000–1100 cm^{-1} (υ3), and OH modes at 630 and 3560 cm^{-1};[48,49] at 620 and 530 cm^{-1},[50] at 960 cm^{-1} (υ1), 430–450 cm^{-1} (υ2), 1040–1074 cm^{-1} (υ3), and 590–608 cm^{-1} (υ4) modes of PO$_4$;[51] PO$_3$ at 862, 932, 1196, 1222 cm^{-1} and 629, 661 cm^{-1} stretching of CP.[52] Pyridine modes are reported at 1025–1055 cm^{-1} (CH deformation);[53] at 1637, 1596, 1582, 1445 cm^{-1}.[54–56]

Table 2. Topological parameters of the title compounds RESD and ZLA for selected BCPs.

Compound	BCP	$\rho(r)$ (a.u)	$\nabla^2\rho(r)$ (a.u)	$V(r)$ (a.u)	$G(r)$ (a.u)	$H(r)$ (a.u)	$-G/V$	ε	ΔE_{HB} (kcal/mol)
RESD	P2–O9	0.177	0.945	−0.440	0.338	−0.102	0.769	0.040	–
	P1–O8	0.171	0.844	−0.412	0.311	−0.100	0.756	0.003	–
	P1–O5	0.147	0.580	−0.316	0.230	−0.086	0.729	0.092	–
	P1–O4	0.141	0.531	−0.293	0.213	−0.080	0.726	0.092	–
	P2–O6	0.139	0.515	−0.288	0.209	−0.080	0.723	0.040	–
	P2–O7	0.129	0.366	−0.249	0.170	−0.079	0.684	0.129	–
	O7–H24	0.061	0.130	−0.076	0.054	−0.022	0.713	0.039	–
	O8–H20	0.054	0.105	−0.062	0.044	−0.018	0.711	0.033	–
	O3–H21	0.016	0.075	−0.014	0.016	0.002	1.174	0.412	−4.36
	O4–C15	0.011	0.046	−0.009	0.010	0.001	1.159	0.746	–
ZLA	P1–O8	0.167	0.617	−0.374	0.264	−0.110	0.706	0.027	–
	P2–O9	0.168	0.605	−0.375	0.263	−0.112	0.702	0.015	–
	P2–O6	0.127	0.261	−0.222	0.144	−0.078	0.647	0.013	–
	P1–O4	0.132	0.247	−0.232	0.147	−0.085	0.633	0.048	–
	P2–O7	0.131	0.233	−0.228	0.143	−0.085	0.628	0.134	–
	P1–O5	0.122	0.218	−0.205	0.130	−0.075	0.633	0.124	–
	O5–H25	0.027	0.097	−0.025	0.025	0.000	0.981	0.149	–
	O3–H22	0.024	0.082	−0.022	0.021	−0.001	0.975	0.198	−6.76
	N10–H19	0.018	0.069	−0.015	0.016	0.001	1.089	2.187	−4.55
	O6–H17	0.016	0.063	−0.013	0.014	0.001	1.111	0.135	−4.00
	O8–H21	0.011	0.039	−0.008	0.009	0.001	1.142	0.109	−2.39

3.3. Aim analysis

Several chemical processes are described using the AIM analysis, which is based on structural properties of charge distribution. According to this theory, every pair of atoms in a molecule system does have its own crucial stage, referred to as the bond critical point (BCP), which has been used to deduce chemical interactions in molecular structures. In this present work, electron density (ED) $\rho(r)$, ED of Laplacian $\nabla^2\rho(r)$, potential energy density $V(r)$, local energy density $H(r)$, kinetic energy density $G(r)$, the ratio of –(G/V) and ellipticity (ε), of RES and ZLA for selected BCPs are determined and are listed in Table 2. Figure 2(a,b) exhibits the AIM molecular maps of the RES and ZLA, respectively. The BCP's (very small green spheres), bond paths (black solid lines), ring critical points RCP's (small red spheres), ring path (solid lines in ash color), non-covalent weak interactions (dotted black lines) are also represented in these figures. Closed-shell and shared interactions between BCPs are usually distinguished using the Laplacian electron density $\nabla^2\rho(r)$ and electron density $\rho(r)$ values.

In this case, the smallest values of $\rho(r)$ and corresponding positive values of $\nabla^2\rho(r)$ of RES and ZLA shown that the closed-shell interactions (Van der Walls and Intra molecular H-bonds) existed in the chemicals at O4–C15 and O3–H21 (RES); at O8–H21, O3–H22, N10–H19, and O6–H17 (ZLA), respectively, and they are shown in Table 2. Other $\nabla^2\rho(r)$ and $\rho(r)$ values of BCPs suggest that shared covalent interactions of the compounds. The maximum bond ellipticity (ε) values are found for RES and ZLA at O4–C15 and N10–H19, respectively, which reflects the anisotropy of electron density curvature of RES and ZLA.[57,58]

The calculated $\nabla^2\rho(r)$ and $H(r)$ are also utilized to classify hydrogen bond interactions further, such as (i) $\nabla^2\rho(r) < 0$ and $H(r) < 0$ for the strong hydrogen bonds and covalent in nature, (ii) $\nabla^2\rho(r) > 0$ and $H(r) < 0$ for intermediate hydrogen bonds and partially covalent and (iii) $\nabla^2\rho(r) > 0$ and $H(r) > 0$ for weak hydrogen bonds electrostatic and non-covalent nature. In this case, the three weak hydrogen bonds (N10–H19, O6–H17, and O8–H21) and one intermediate hydrogen bond (O3–H22) were confirmed in the ZLA compound by the $\nabla^2\rho(r)$ and $H(r)$ values. Similarly one weak H-bond (O3–H21) was found for the compound RES. These H-bonds interaction energies ($\Delta E_{X\cdots H}$) were also calculated by half of the potential energy density $V(r)$ at corresponding BCPs ($E_{X\cdots H} = V(r)/2$),[59,60] and the highest interaction energy was found at O3···H22 (−6.76 kcal/mol). In addition, the ratio $-(G/V)$, demonstrated the non-covalent character of these interactions.
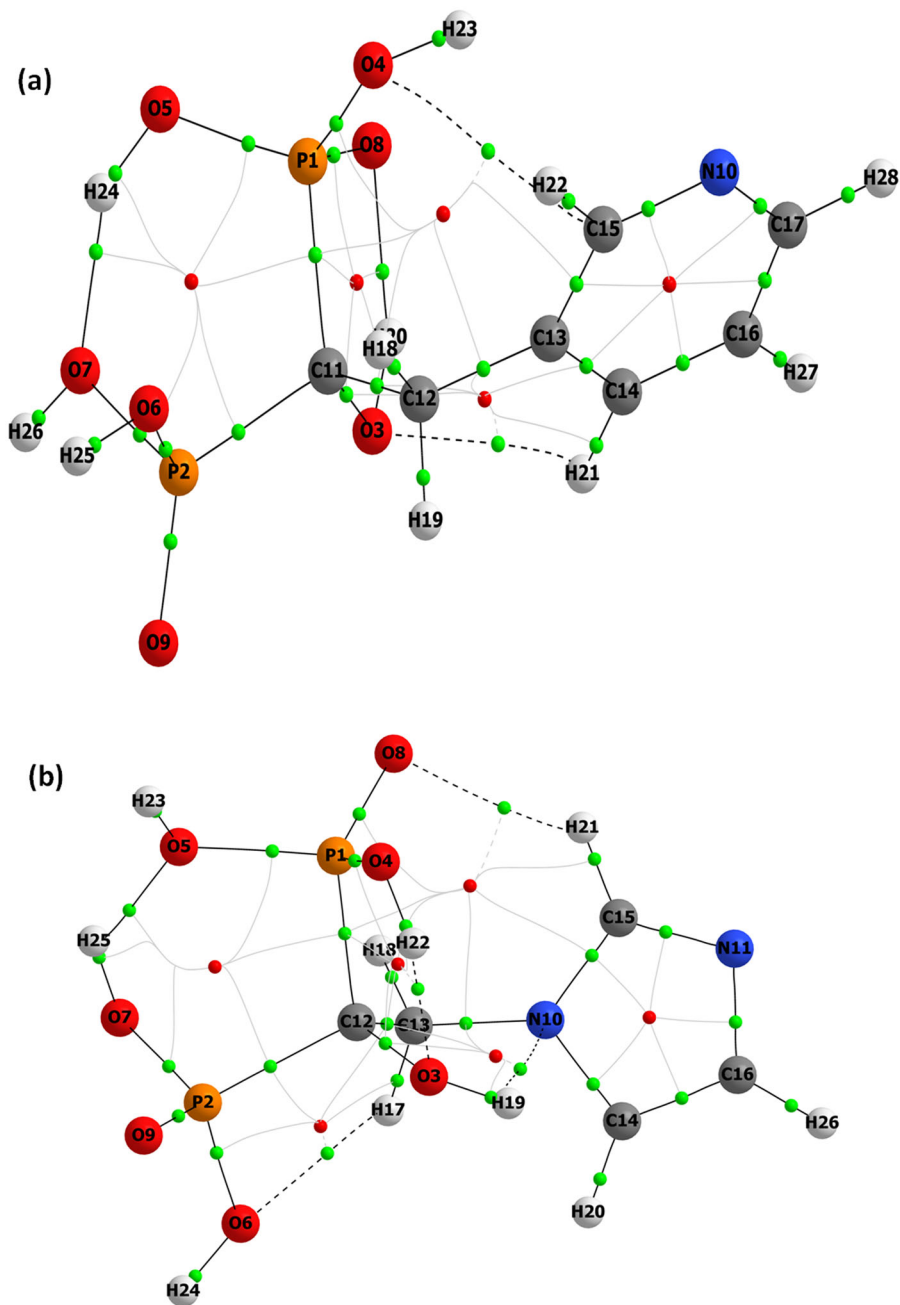
Figure 2. AIM Molecular graph of (a) RES and (b) ZLA: a green small spheres (BCPs), small red sphere (RCBs), black lines (bond paths), ash color solid lines (RCP to BCP ring path), block dotted lines (non-covalent weak interactions).

3.4. LOL and ELF

The ELF and LOL were commonly employed to show the relationships between electrical and geometric structures, as well as to better comprehend the bond kinetics of the molecules' main bioactive sites. In this work, the two chemicals of RES and ZLA are investigated by ELF and LOL analysis for topological properties of the substances. In Figures 3 and 4, the color red signifies a region with strong ELF and LOL values, while the color blue indicates a place with weak ELF
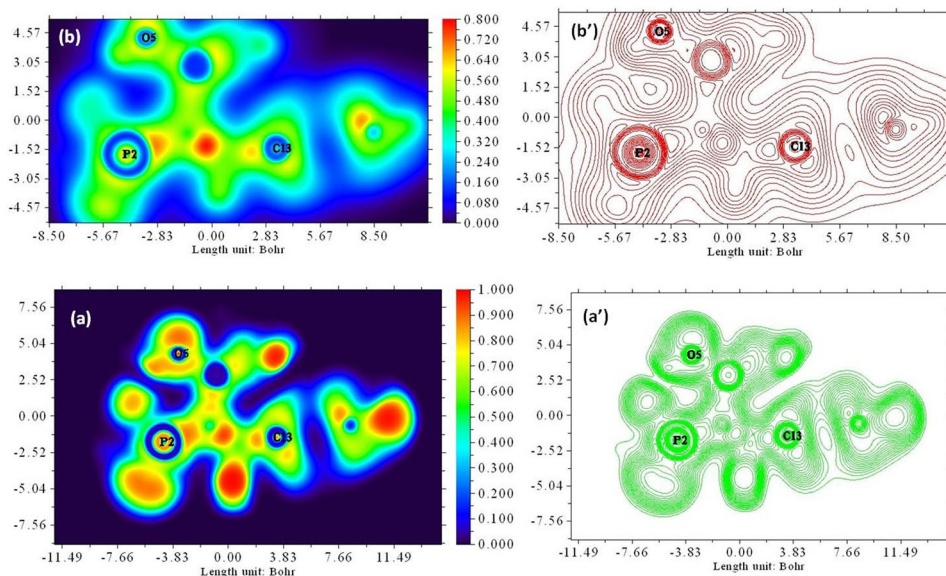
Figure 3. (a,a′) Electron localization function (ELF) and (b,b′) Localized orbital locator (LOL) maps and contour surfaces of RES.

and LOL values of RES and ZLA, respectively. The color red and blue are also used to represent electron localization and delocalization.[61,62] These localized and delocalized atoms and regions are used to describe the chemical structure of the RES and ZLA. In RES and ZLA, the deepest blue rings around P2, O5, and C13 for RES, and P2, C12, C14, and C16 for ZLA, which suggested that these are the strongest delocalized regions of these compounds. The phosphorus and oxygen atoms are more delocalized due to its electron withdrawing inductive effect and lone pair of resonance effect at P1 and P2 of RES and P2 of ZLA, whereas the carbon atoms (C13 for RES and C14 and C16 for ZLA) also delocalized due to π electrons of aromatic ring by resonance. The highest delocalization zones are around the few number of nuclei among them, and their related chemical environment O7–P2–O9, O5–P1–O4, and C15–C13–C14 (for RES); and O7–P2–O9, P2–C12–O3, and N10–C14–C16 (for ZLA), which are graphically illustrated in Figure S3 and S4. The P and C atoms were more strongly delocalized and there were more delocalized regions presented in RES when compared to ZLA.

3.5. RDG analysis

In this study on RES and ZLA, the RDG map was utilized to find weak interactions between atoms in a molecule, such as intra molecular hydrogen bonds, van der Waals connections, and steric effects. The NCI-RDG graph is constructed by plotting RDG versus sign $(\lambda_2)\rho$ to highlight these weak interactions in a very small range.[63–65] In this graph (Figure 5), the sign $(\lambda_2)\rho$ regions of red color spikes denotes a strong steric repulsive effect; the green color spikes reveals Van der walls interactions at O3–H21 for compound RES; and the blue regions (and spikes) represent the hydrogen bond connections. In the present case, Figure 5(a,b) shows that the weak interactions between the molecular groups of RES and ZLA respectively, the region of sign $(\lambda_2)\rho$ at green color spikes (−0.01 to −0.02 a.u. for RES; −0.01 to −0.02 a.u. for ZLA) represent the same Van der walls interactions in both two molecules; the red color spikes (0.01–0.03 a.u. for RES; 0.01–0.02 a.u. for ZLA) indicates that the strong steric repulsive effect in RES than ZLA and also this plot shows, the blue regions (−0.03 to −0.05 a.u. for RESD; −0.025 to −0.029 a.u. for ZLA) was confirmed that the intra molecular weak hydrogen bond interactions of compounds (at
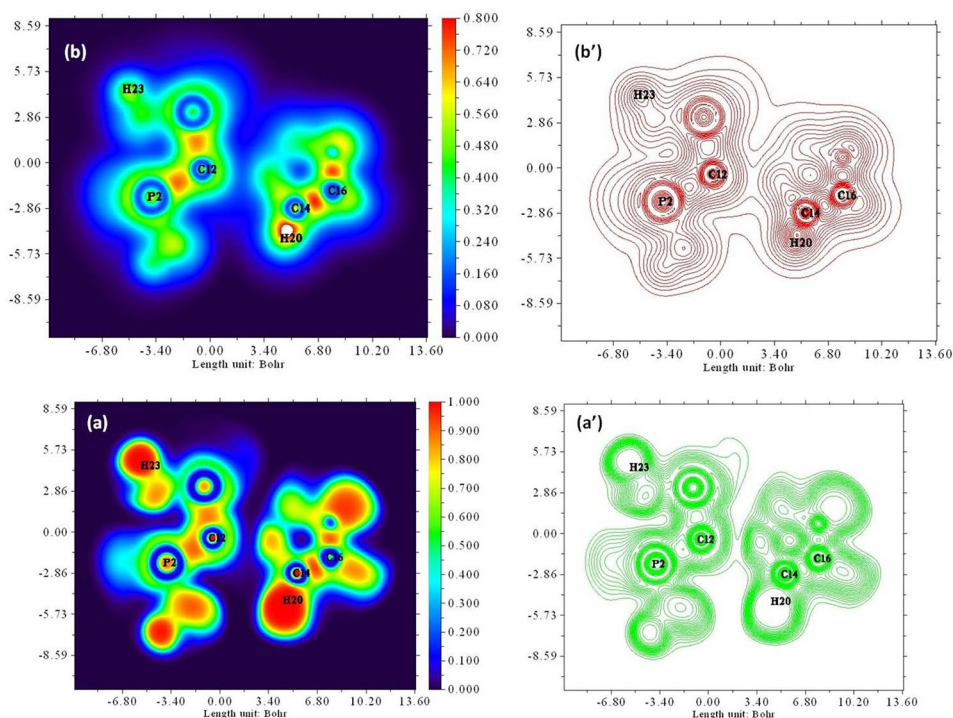
Figure 4. (a,a') Electron localization function (ELF) and (b,b') Localized orbital locator (LOL) maps and contour surfaces of ZLA.
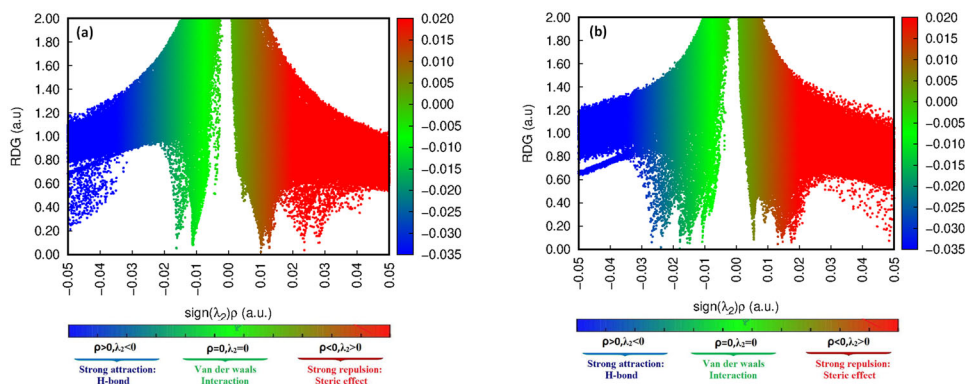

Figure 5. RDG Plots versus the electron density ρ multiplied by the sign of λ_2 for (a) RESD and (b) ZLA.

O4–C15 for RES and O8–H21, O3–H22, N10–H19, and O6–H17 for ZLA). Since the results of this study (sign $(\lambda_2)\rho$ values) suggests that the four intra molecular hydrogen bonds in the ZLA compound are weak and their interaction energies are slightly greater than RES, and the results of earlier AIM calculations of the H-bond interactions were validated by this conclusion.

3.6. Molecular modeling, docking, and dynamics

AI/ML-based modeling of Wnt5A in Alpha fold displayed a convincing model (S5a) with a DOPE score −2.67 and in Ramachandran plot the phi and psi dihedral angles mostly lying in the most favored regions >94%, 0.6% additionally allowed and 0.3% generally allowed regions
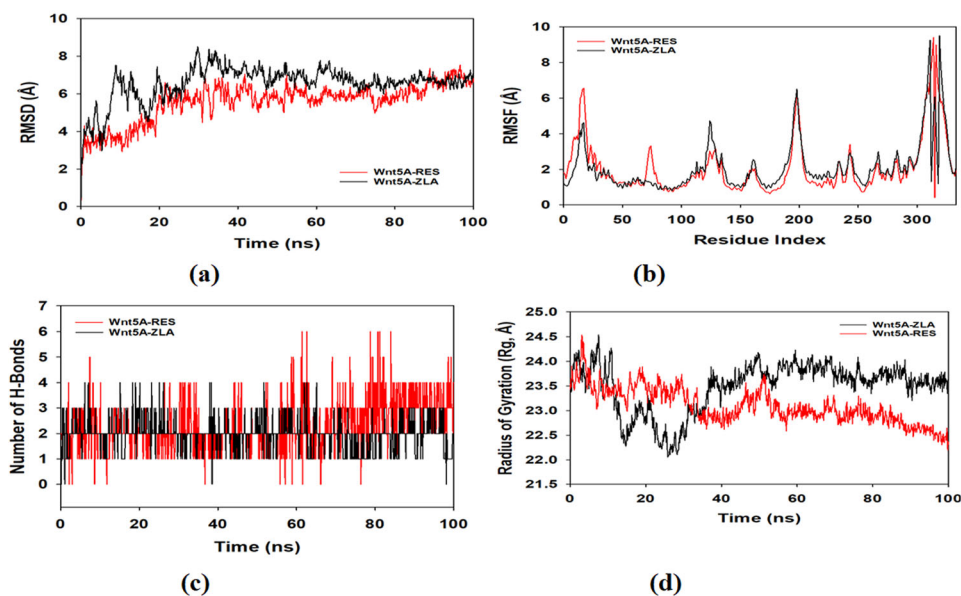
Figure 6. (a) RMSD of protein and ligands; (b) RMSF of protein and ligands; (c) hydrogen bonds; (d) radius of gyration.

(Figure S5(a)). From Ramachandran plot, it can be suggested that the protein is of high quality. Quality assessment results of modeled Wnt5A by ProSA web results showed that the modeled protein was positioned in both X-ray and NMR regions with a score −7.42 (Figure S5(b), Good quality structures usually lie within the regions of X-ray and NMR). On the other hand, Errat plot displayed overall quality factor of the modeled Wnt5A is 97.973. Two lines are shown on the error axis to illustrate the confidence with which regions that exceed the error value can be rejected. It was observed from Figure S5(c), that most of the residues lay in the good confidence level with least error. Therefore, homology modeling and quality assessment of the model suggested that the modeled protein is of good quality.

Molecular interaction studies in between the modeled protein Wnt5A and ligands ZLA and RES were carried out to determine the predicted binding energy score (ΔG) and inhibitory concentration (Ki). Docking studies revealed that the ZLA ligand bound convincingly to a pocket in the Wnt5A protein with lowest binding energy −7.8 kcal/mol with Ki −6.0 μM. The principal amino acid residues involved in ligand binding GLN107, ARG109, HIS110, and ARG111 are involved in making conventional hydrogen bond (Figure S5(d)), While ASP271 attractive charge interaction. On the other hand, RES ligand bound comparatively high affinity with Wnt5A than ZLA with lowest binding energy with a RMSD tolerance 0.25 Å and having highest numbers of clusters in this tolerance limit. The binding energy was predicted to be −8.1 kcal/mol with inhibitory concentration (Ki) −2.4 μM. The principle residues at binding pocket of Wnt5A are THR99, GLU103, and ARG260 involving in conventional hydrogen bonds with RES ligand. Therefore, it can be suggested that ligand RES perhaps better choice for lead identification for future bone cancer therapy. RES docked with New Delhi metallo-β-lactamase-1 with a score of −10.54 kcal/mol.[66]

MD and simulation of the ligand bound main WNT5A were studied in details to understand the nature of possible binding motifs and structurally stable conformations. In order to obtain the information of accurate structural convergence in MD studies, replication of the simulations were done using same system parameters. The RMSD of 100 ns simulation trajectories displayed a stable conformation of the complex (Figure 6(a), red and black) complex with 0.5 Å deviations, while the ligand RMSD also displayed very less deviation indicating the stable complex with WNT5A.[67] Root mean square fluctuations of the whole C-alpha atom of WNT5A-RES and
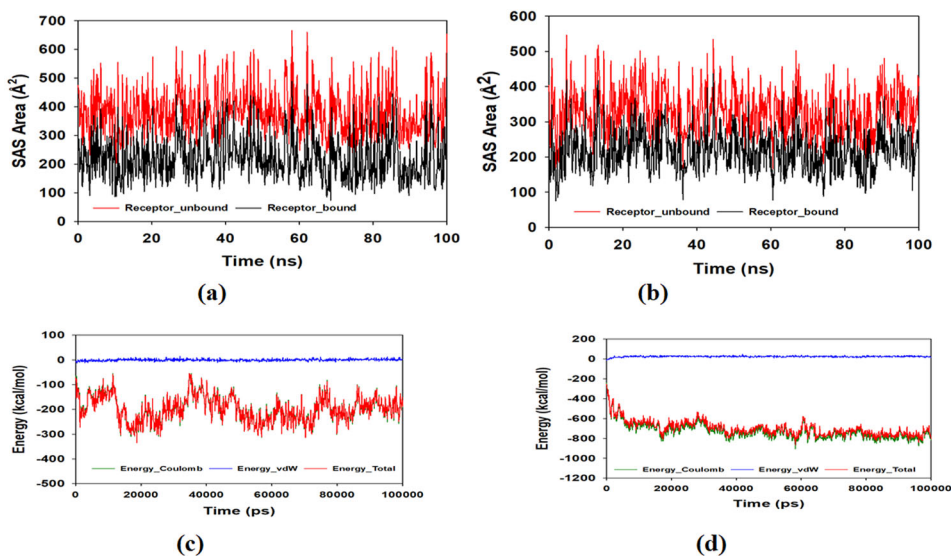
Figure 7. (a) SASA Values of WNT5A-RES Complex (b) SASA Values of WNT5A-ZLA Complex (c) Total Energy WNT5A-RES (d) Total Energy WNT5A-ZLA.

WNT5A-ZLA at a function of 100 ns time scale displayed very less deviations except at 311 residue position (7.4 and 9.2 Å) indicating very stable and compact protein ligand complex (Figure 6(b)).[68]

The number of hydrogen bonds (Figure 6(c)) formed throughout the simulations was found to be 6 for WNT5A-RES complex and 4 for WNT5A-ZLA complex. Radius of Gyration (Figure 6(d)) of C-alpha atom of WNT5A displayed the conformational convergence toward a compact structure leading to stable WNT5A-Ligand complexes which is also in agreement with RMSF values. The binding SASA (Figure 7(a,b)) displayed lowering of surface area in the complex as compared to unbound protein structure. This indicates compactness of the ligand bound protein complex and suggesting an equilibrated as well as converged structure. Since the process was done for 100 ns and both shows a steady SASA values for WNT5A-RES complex from 60 to 100 ns around 299.65–654.17 (A^2) for unbound and 144.17–502.81 (A^2) for the bound structures and WNT5A-ZLA complex from 60 to 100 ns around 258.84–423.08 (A^2) for unbound and 158.44–301.47 (A^2) for the bound structures.[69,70]

The total energy (Figure 7(c,d)) of the whole system is found to be very stable and minimized global energy. The two major non bonded interactions played important role in stabilizing the complex such as Van der Waals and Coulomb energy. The Coulomb energy displayed high contribution to achieve a global minima structure of whole complex throughout simulation time of 100 ns as compared to Van der Waals energy.

4. Conclusion

The SFE (water/DMSO) are −29.61/−19.33 for RES and −26.85/−22.55 kcal/mol for ZLA which supports the biological activity. In solvents deviations are observed for the vibrational modes and geometrical parameters. FMOs energies and HOMO-LUMO gap calculated for RES/ZLA are somewhat lower in solution, indicating that the dielectric constant changes reactivity of RES/ZLA, directly affecting the reactivity indexes, revealing lower values for hardness and electrophilicity index in solvents. In this investigation, for RES and ZLA, the RDG map was utilized to find weak interactions between atoms in a molecule, such as intramolecular hydrogen bonds, van der Waals

connections, and steric effects. Homology modeling and quality assessment of the model suggested that the modeled protein is of good quality. The intramolecular hydrogen bonds in the ZLA compound are weak and their interaction energies are slightly greater than RES. At the binding pocket of the receptor, the presence of principle residues suggests that RES is a better choice for lead identification for future bone cancer therapy than ZLA. The steady SASA values of RES are greater than that of ZLA which support the above argument.

Acknowledgments

Disclosure statement

Funding

References

1. P. Wu, D.J. Siegwart, and H. Xiong, "Recent Advances in the Targeted Fluorescent Probes for the Detection of Metastatic Bone Cancer," *Science China Chemistry* 64, no. 8 (2021): 1283–96. https://doi.org/10.1007/s11426-021-9990-x

2. A.S. Andriessen, C.R. Donnelly, and R.R. Ji, "Reciprocal Interactions between Osteoclasts and Nociceptive Sensory Neurons in Bone Cancer Pain," *Pain Reports* 6, no. 1 (2021): e867. https://doi.org/10.1097/pr9.0000000000000867

3. J.A. Paice, M. Mulvey, M. Bennet, P.M. Dougherty, J.T. Farrar, P.W. Mantyh, C. Miaskowski, B. Schmidt, and T.J. Smith, "AAPT Diagnostic Criteria for Chronic Cancer Pain Conditions," *The Journal of Pain* 18, no. 3 (2017): 233–46. https://doi.org/10.1016/j.jpain.2016.10.020

4. T. Tian, W.T. Yang, H. Wang, S. Dang, and Z.M. Sun, "Flexible Diphosphonic Acids for the Isolation of Uranyl Hybrids with Heterometallic U^{VI} =O-Zn^{II} Cation-Cation Interactions," *Inorganic Chemistry* 52, no. 15 (2013): 8288–90. https://doi.org/10.1021/ic4009834

5. A.N. Kozachkova, N.V. Tsaryk, A.V. Dudko, V.I. Pekhnyo, V.M. Novotortsev, I.L. Eremenko, V.V. Minin, N.N. Efimov, and E.A. Ugolkova, "Crystal Structure and Magnetic Properties of a New Heterometallic Complex of Pd(II)-Cu(II) with 1-Aminoethylidene-1,1-Diphosphonic Acid," *Journal of Structural Chemistry* 54, no. 2 (2013): 315–20. https://doi.org/10.1134/S0022476613020066

6. S. M.F. Vilela, R. F. Mendes, P. Silva, J. A. Fernandes, J. P.C. Tomé, and F.A.A. Paz, "Structural Diversity of Lanthanum-Organic Frameworks Based on1,4-Phenylenebis(Methylene)Phosphonic Acid," *Crystal Growth and Design* 13, no. 2 (2013): 543–60. https://doi.org/10.1021/cg301112k

7. C. Xie, Q.R. Cheng, and Z.Q. Pan, "Hydrothermal Synthesis and Crystal Structure of Alkaline Earth Metal (Mg,Ca) Based on 2,5-Dimethylbenzene-1,4-Diylbis (Methylene)Diphosphonic Acid," *Journal of Molecular Structure* 1154 (2018): 232–8. https://doi.org/10.1016/j.molstruc.2017.10.036

8. K. Gholivand, N. Fallah, A.A.E. Valmoozi, A. Gholami, M. Dusek, V. Eigner, M. Pooyan, and F. Mohammadpanah, "Synthesis and Structural Characterization of Phosphinate Coordination Polymers with Tin(IV) and Copper(II)," *Journal of Molecular Structure* 1202 (2020): 127369. https://doi.org/10.1016/j.molstruc.2019.127369

9. Z. Nikfar, and Z. Shariatinia, "DFT Computational Study on the Phosphate Functionalized SWCNTs as Efficient Drug Delivery Systems for Anti-Osteoporosis Zolendronate and Risedronate Drugs," *Physica E: Low-Dimensional Systems and Nanostructures* 91 (2017): 41–59. https://doi.org/10.1016/j.physe.2017.04.011

10. P. L. Minciullo, A. Allegra, A. D'Angelo, C. Musolino, and S. Gangemi, "Challenge Test to Bisphosphonates in Patients with Hypersensitivity Reactions to Drugs," *Allergologia et Immunopathologia* 43, no. 2 (2015): 127–30. https://doi.org/10.1016/j.aller.2013.09.010

11.   Y.H. Kao, L.C. Chang, Y.W. Tsai, L.K. Chen, and W.F. Huang, "Risk and Cost Effectiveness Analysis of Adverse Atrial Fibrillation Outcome in Treating Osteroprosis," *Value in Health* 16, no. 3 (2013): A217. https://doi.org/10.1016/j.jval.2013.03.1102

12.   D.K. Khajuria, C. Disha, R. Vasireddi, R. Razdan, and D.R. Mahapatra, "Risedronate/Zinc-Hydroxyapatite Based Nanomedicine for Osteoporosis," *Materials Science & Engineering C, Materials for Biological Applications* 63 (2016): 78–87. https://doi.org/10.1016/j.msec.2016.02.062

13.   S. Mosbahi, H. Oudadesse, B. Lefeuvre, A. Barroug, H. Elfeki, A. Elfeki, C. Roiland, and H. Keskes, "Risedronate Adsorption on Bioactive Glass Surface for Applications as Bone Biomaterial," *Applied Surface Science* 367 (2016): 205–13. https://doi.org/10.1016/j.apsusc.2016.01.184

14.   K. Koto, H. Murata, S. Kimura, N. Horie, T. Matsui, Y. Nishigaki, K. Ryu, T. Sakabe, M. Itoi, E. Ashihara, et al., "Zoledronic Acid Inhibits Proliferation of Human Fibrosarcoma Cells with Induction of Apoptosis and Shows Combined Effects with Other Anticancer Agents," *Oncology Reports* 24, no. 1 (2010): 233–9. https://doi.org/10.3892/or_00000851[PMC][20514467

15.   A. Migliore, S. Broccoli, U. Massafra, E. Bizzi, and B. Frediani, "Mixed Treatment Comparison of Anabolic(Teriparatide and PTH 1-84) Therapies in Women with Severe Osteoporosis," *Current Medical Research and Opinion* 28, no. 3 (2012): 467–73. https://doi.org/10.1185/03007995.2012.659724

16.   A. Dokoutchaev, V. V. Krishnan, M. E. Thompson, and M. Balasubramanian, "Platinum and Palladium Incorporation into Phosphate/Viologen-Phosphonates of Zirconium and Hafnium: Synthesis and Characterization," *Journal of Molecular Structure* 470, no. 1–2 (1998): 191–205. https://doi.org/10.1016/S0022(98)00481-5

17.   H. Sakai, T. Kubota, J. Yuasa, Y. Araki, T. Sakanoue, T. Takenobu, T. Wada, T. Kawai, and T. Hasobe, "Protonation Induced Red Coloured Circularly Polarized Luminescence of [5]Carbohelicene Fused by Benzimidazole," *Organic & Biomolecular Chemistry* 14, no. 28 (2016): 6738–43. https://doi.org/10.1039/C6OB00937A

18.   R.C. Lirag, H.T.M. Le, and O.S. Miljanic, "L-Shaped Benzimidazole Fluorophores: Synthesis, Characterization and Optical Response to Bases, Acids and Anions," *Chemical Communications* 49, no. 39 (2013): 4304–6. https://doi.org/10.1039/C2CC37120K

19.   A.T. Myller, J.J. Karhe, M. Haukka, and T.T. Pakkanen, "The pH Behavior of a 2-Aminoethyl Dihydrogen Phosphate Zwitterion Studied with NMR-Titrations," *Journal of Molecular Structure* 1033 (2013): 171–5. https://doi.org/10.1016/j.molstruc.2012.08.033

20.   Y. Shao, Q. Zheng, W. Wang, N. Xin, X. Song, and C. Zhao, "Biological Functions of Macrophage-Derived Wnt5a and Its Roles in Human Disease," *Oncotarget* 7, no. 41 (2016): 67674–84. https://doi.org/10.18632/oncotarget.11874

21.   S.J. Armakovic, Y.S. Mary, Y.S. Mary, S. Pelemis, and S. Armakovic, "Optoelectronic Properties of the Newly Designed 1,3,5-Triazine Derivatives with Isatin, Chalcone and Acridone Moieties," *Computational and Theoretical Chemistry* 1197 (2021): 113160. https://doi.org/10.1016/j.comptc.2021.113160

22.   G. Venkatesh, C. Kamal, P. Vennila, M. Govindaraju, Y.S. Mary, S. Armakovic, S.J. Armakovic, S. Kaya, and C.Y. Panicker, "Molecular Dynamic Simulations, ALIE Surfaces, Fukui Functions, Geometrical, Molecular Docking and Vibrational Spectra Studies of Tetra Chlorop and m-Xylene," *Journal of Molecular Structure* 1171 (2018): 253–67. https://doi.org/10.1016/j.molstruc.2018.06.001

23.   L. Ouksel, S. Chafaa, R. Bourzami, N. Hamdouni, M. Sebais, and N. Chafai, "Crystal Structure, Vibrational, Spectral Investigation, Quantum Chemical DFT Calculations and Thermal Behavior of Diethyl[Hydroxyl(Phenyl)Methyl]Phosphonate," *Journal of Molecular Structure* 1144 (2017): 389–95. https://doi.org/10.1016/j.molstruc.2017.05.029

24.   A. Hellal, S. Chafaa, N. Chafai, and L. Touafri, "Synthesis, Antibacterial Screening and DFT Studies of a Series of α-Aminophosphonates Derivatives from Amino-Phenols," *Journal of Molecular Structure* 1134 (2017): 217–25. https://doi.org/10.1016/j.molstruc.2016.12.079

25.   M.J. Frisch, G.W. Trucks, H.B. Schlegel, G.E. Scuseria, M.A. Robb, J.R. Cheeseman, G. Scalmani, V. Barone, B. Mennucci, G.A. Petersson, et al., *Gaussian 09, Revision B.01* (Wallingford CT: Gaussian Inc., 2010).

26.   R. Dennington, T. Keith, and J. Millam, *Gaussview, Version 5* (Shawnee Mission, KS: Semichem Inc., 2009).

27.   T.A. Keith, *AIMAll Version 19.10.12* (Overland Park, KS: TKGristmill Software, 2019).

28.   E. R. Johnson, S. Keinan, P. Mori-Sánchez, J. Contreras-García, A. J. Cohen, and W. Yang, "Revealing Noncovalent Interactions," *Journal of the American Chemical Society* 132, no. 18 (2010): 6498–506. https://doi.org/10.1021/ja100936w

29.   J. Jumper, R. Evans, A. Pritzel, T. Green, M. Figurnov, O. Ronneberger, K. Tunyasuvunakool, R. Bates, A. Žídek, A. Potapenko, et al., "Highly Accurate Protein Structure Prediction with AlphaFold," *Nature* 596, no. 7873 (2021): 583–9. https://doi.org/10.1038/s41586-021-03819-2

30.   M. Wiederstein, and M.J. Sippl, "ProSA-Web: Interactive Web Service for the Recognition of Errors in Three-Dimensional Structures of Protein," *Nucleic Acids Research* 35 (2007): W407–W410. https://doi.org/10.1093/nar/gkm290

31. R.A. Laskowski, M.W. MacArthur, D.S. Moss, and J.M. Thornton, "PROCHECK: A Program to Check the Stereochemical Quality of Protein Structures," *Journal of Applied Crystallography* 26, no. 2 (1993): 283–91. https://doi.org/10.1107/S0021889892009944

32. G.M. Morris, R. Huey, W. Lindstrom, M.F. Sanner, R.K. Belew, D.S. Goodsell, and A.J. Olson, "Autodock4 and AutodockTools4: Automated Docking with Selective Receptor Flexibility," *Journal of Computational Chemistry* 30, no. 16 (2009): 2785–91. https://doi.org/10.1002/jcc.21256

33. K.J. Bowers, D.E. Chow, H. Xu, R.O. Dror, M.P. Eastwood, B.A. Gregersen, J.L. Klepeis, I. Kolossvary, M.A. Moraes, F.D. Sacerdoti, et al., "Scalable Algorithms for Molecular Dynamics Simulations on Commodity Clusters" (InSc'06: Proceedings of the 2006 ACM/IEEE Conference on Supercomputing, 2006).

34. E. Chow, C.A. Rendleman, K.J. Bowers, R.O. Dror, D.H. Hughes, J. Gullingsrud, F.D. Sacerdoti, and D.E. Shaw, "Desmond Performance on a Cluster of Multicore Processors" (DE Shaw Research Technical Report DESRES/TR—2008-01, 2008).

35. D. Shivakumar, J. Williams, Y. Wu, W. Damm, J. Shelley, and W. Sherman, "Prediction of Absolute Solvation Free Energies Using Molecular Dynamics Free Energy Perturbation and the OPLS Force Field," *Journal of Chemical Theory and Computation* 6, no. 5 (2010): 1509–19. https://doi.org/10.1021/ct900587b

36. W.L. Jorgensen, J. Chandrasekhar, J.D. Madura, R.W. Impey, and M.L. Klein, "Comparison of Simple Potential Functions for Simulating Liquid Water," *The Journal of Chemical Physics* 79, no. 2 (1983): 926–35. https://doi.org/10.1063/1.445869

37. G.J. Martyna, D.J. Tobias, and M.L. Klein, "Constant Pressure Molecular Dynamics Algorithms," *Journal of Chemical Physics* 101, no. 5 (1994): 4177–89. https://doi.org/10.1063/1.467468

38. G.J. Martyna, J.M.L. Klein, and M. Tuckerman, "Nose-Hoover Chains-the Canonical Ensemble via Continuous Dynamics," *Journal of Chemical Physics* 97, no. 4 (1992): 2635–43. https://doi.org/10.1063/1.463940

39. A.Y. Toukmaji, and J.A. Board, Jr., "Ewald Summation Techniques in Perspective: A Survey," *Computer Physics Communications* 95, no. 2–3 (1996): 73–92. https://doi.org/10.1016/0010-4655(96)00016-1

40. A.V. Marenich, C.J. Cramer, and D.G. Truhlar, "Universal Solvation Model Based on Solute Electron Density and on a Continuum Model of the Solvent Defined by the Bulk Dielectric Constant and Atomic Surface Tensions," *The Journal of Physical Chemistry B* 113, no. 18 (2009): 6378–96. https://doi.org/10.1021/jp810292n

41. G.D.R. Matos, D.Y. Kyu, H.H. Loeffler, J.D. Chodera, M.R. Shirts, and D.L. Mobley, "Approaches for Calculating Solvation Free Energies and Enthalpies Demonstrated with an Update of the FreeSolv Database," *Journal of Chemical and Engineering Data* 62, no. 5 (2017): 1559–69. https://doi.org/10.1021/acs.jced.7b00104

42. J.G.O. Marques, A.L. Costa, and C. Pereira, "Gibbs Free Energy (ΔG) Analysis for the Na-O-H (Sodium-Oxygen-Hydrogen) Thermochemical Water Splitting Cycle," *International Journal of Hydrogen Energy* 44, no. 29 (2019): 14536–49. https://doi.org/10.1016/j.ijhydene.2019.04.064

43. J.S. Al-Otaibi, A.H. Almuqrin, Y.S. Mary, and Y.S. Mary, "Comprehensive Quantum Mechanical Studies on Three Bioactive Anastrozole Based Triazole Analogues and Their SERS Active Graphene Complex," *Journal of Molecular Structure* 1217 (2020): 128388. https://doi.org/10.1016/j.molstruc.2020.128388

44. P. Vennila, M. Govindaraju, G. Venkatesh, C. Kamal, Y.S. Mary, C.Y. Panicker, S. Kaya, S. Armakovic, and S.J. Armakovic, "A Complete Computational and Spectroscopic Study of 2-Bromo-1,4-dichlorobenzene-A Frequently Used Benzene Derivative," *Journal of Molecular Structure* 1151 (2018): 245–55. https://doi.org/10.1016/j.molstruc.2017.09.049

45. K. O. Rachedi, T. S. Ouk, R. Bahadi, A. Bouzina, S. E. Djouad, K. Bechlem, R. Zerrouki, T. Ben Hadda, F. Almalki, and M. Berredjem, "Synthesis, DFT and POM Analyses of Cytotoxicity Activity of α-Amidophosphonates Derivatives: Identification of Potential Antiviral O,O-Pharmacophore Site," *Journal of Molecular Structure* 1197 (2019): 196–203. https://doi.org/10.1016/j.molstruc.2019.07.053

46. B. Sureshkumar, Y.S. Mary, K.S. Resmi, C.Y. Panicker, S. Armakovic, S.J. Armakovic, C. Van Alsenoy, B. Narayana, and S. Suma, "Spectroscopic Analysis of 8-Hydroxyquinoline Derivatives and Investigation of Its Reactive Properties by DFT and Molecular Dynamics Simulations," *Journal of Molecular Structure* 1156 (2018): 336–47. https://doi.org/10.1016/j.molstruc.2017.11.120

47. N.P.G. Roeges, *A Guide to the Complete Interpretation of Infrared Spectra of Organic Structures* (New York, NY: John Wiley and Sons Inc., 1994).

48. J.C. Elliott, *Structure and Chemistry of Apatites and Other Calcium Ortho Phosphates* (Amsterdam, Netherlands: Elsevier, 1994).

49. F. Errassifi, S. Sarda, A. Barroug, A. Legrouri, H. Sfihi, and C. Rey, "Infrared, Raman and NMR Investigations of Risedronate Adsorption on Nanocrystalline Apatites," *Journal of Colloid and Interface Science* 420 (2014): 101–11. https://doi.org/10.1016/j.jcis.2014.01.017

50. C. Rey, C. Combes, C. Drouet, S. Cazalbou, D. Grossin, F. Brouillet, and S. Sarda, "Surface Properties of Biomimetic Nanocrystalline Apatites: Applications in Biomaterials," *Progress in Crystal Growth and Characterization of Materials* 60, no. 3–4 (2014): 63–73. https://doi.org/10.1016/j.pcrysgrow.2014.09.005

51. C. Combes, S. Cazalbou, and C. Rey, "Apatitle Biominerals," *Minerals* 6, no. 2 (2016): 34. https://doi.org/10.3390/min6020034

52. I. Cukrowski, L. Popovic, W. Barnard, S.O. Paul, P.H. van Rooyen, and D.C. Liles, "Modeling and Spectroscopic Studies of Bisphosphonate-Bone Interactions: The Raman, NMR and Crystallographic Investigations of a CA-HEDP Complexes," *Bone* 41, no. 4 (2007): 668–78. https://doi.org/10.1016/j.bone.2007.05.008

53. N. Redman-Furey, M. Dicks, A. Bigalow-Kern, R.T. Cambron, G. Lubey, C. Lester, and D. Vaughn, "Structural and Analytical Characterization of Three Hydrates and an Anhydrate Form of Risedronate," *Journal of Pharmaceutical Sciences* 94, no. 4 (2005): 893–911. https://doi.org/10.1002/jps.20308

54. C. Lester, G. Lubey, M. Dicks, G. Andol, D. Vaughn, R.T. Cambron, K. Poiesz, and N. Redman-Furey, "Dehydration of Risedronate Hemi-Pentahydrate: Analytical and Physical Characterization," *Journal of Pharmaceutical Sciences* 95, no. 12 (2006): 2631–44. https://doi.org/10.1002/jps.20662

55. B. Demoro, F. Caruso, M. Rossi, D. Benítez, M. Gonzalez, H. Cerecetto, B. Parajón-Costa, J. Castiglioni, M. Galizzi, R. Docampo, et al., "Risedronate Metal Complexes Potentially Active against Chagas Disease," *Journal of Inorganic Biochemistry* 104, no. 12 (2010): 1252–8., https://doi.org/10.1016/j.jinorgbio.2010.08.004

56. Q. Liu, L. Qiu, Y. Wang, G. Lv, G. Liu, S. Wang, and J. Lin, "Solvent Effect on Molecular Structure, IR Spectra, Thermodynamic Properties and Chemical Stability of Zoledronic Acid: DFT Study," *Journal of Molecular Modeling* 22, no. 4 (2016): 84. https://doi.org/10.1007/s00894-016-2953-9[PMC][26994018

57. V. S. Kumar, Y.S. Mary, Y.S. Mary, G. Serdaroğlu, A. S. Rad, M.S. Roxy, P.S. Manjula, and B.K. Sarojini, "Conformational Analysis and DFT Investigations of Two Triazole Derivatives and Its Halogenated Substitution by Using Spectroscopy, AIM and Molecular Docking," *Chemical Data Collections* 31 (2021): 100625. https://doi.org/10.1016/j.cdc.2020.100625

58. Y.S. Mary, Y.S. Mary, A.S. Rad, R. Yadav, I. Celik, and S. Sarala, "Theoretical Investigation on the Reactive and Interaction Properties of Sorafenib – DFT, AIM, Spectroscopic and Hirshfeld Analysis, Docking, and Dynamics Simulation," *Journal of Molecular Liquids* 330 (2021): 115652. https://doi.org/10.1016/j.molliq.2021.115652

59. M. Thirunavukkarasu, G. Balaji, S. Muthu, S. Sakthivel, P. Prabakaran, and A. Irfan, "Theoretical Conformations Studies on 2-Acetyl-Gamma-Butyrolactone Structure and Stability in Aqueous Phase and the Salvation Effects on Electronic Properties by Quantum Computational Methods," *Computational and Theoretical Chemistry* 1208 (2022): 113534. https://doi.org/10.1016/j.comptc.2021.113534

60. M. Thirunavukkarasu, G. Balaji, P. Prabakaran, S.J. Basha, A. Irfan, S. Javed, and S. Muthu, "Spectral Characterization, Salvation Effects on Topological Aspects, and Biological Attributes of Fmoc-L-Glutamic Acid 5-Tert-Butyl Ester: An Effective Reagent in Anticancer Evaluations," *Journal of Molecular Structure* 1269 (2022): 133793. https://doi.org/10.1016/j.molstruc.2022.133793

61. A. Saral, P. Sudh, S. Muthu, and A. Irfan, "Computational, Spectroscopic and Molecular Docking Investigations on a Bioactive Anticancer Drug: 2-Methyl-8-Nitroquinoline," *Journal of Molecular Structure* 1247 (2022): 131414. https://doi.org/10.1016/j.molstruc.2021.131414

62. M. Smitha, Y.S. Mary, Y.S. Mary, G. Serdaroglu, P. Chowdhury, M. Rana, H. Umamahesvari, B.K. Sarojini, B.J. Mohan, and R. Pavithran, "Modeling the DFT Structural and Reactivity Studies of a Pyrimidine-6-Carboxylate Derivative with Reference to Its Wavefunction Dependent, MD Simulations and Evaluation for Potential Antimicrobial Activity," *Journal of Molecular Structure* 1237 (2021): 130397. https://doi.org/10.1016/j.molstruc.2021.130397

63. A.F. Basha, F.L.A. Khan, S. Muthu, and M. Raja, "Computational Evaluation on Molecular Structure (Monomer, Dimer), RDG, ELF, Electronic (HOMO-LUMO, MEP) Properties and Spectroscopic Profiling of 8-Quinolinesulfonamide with Molecular Docking Studies," *Computational and Theoretical Chemistry* 1198 (2021): 113169. https://doi.org/10.1016/j.comptc.2021.113169

64. Y.S. Mary, Y.S. Mary, K.S. Resmi, S. Sarala, R. Yadav, and I. Celik, "Modeling the Structural and Reactivity Properties of Hydrazono Methyl-4H-Chromen-4-One Derivatives - Wavefunction-Dependent Properties, Molecular Docking and Dynamics Simulation Studies," *Journal of Molecular Modeling* 27, no. 6 (2021): 186. https://doi.org/10.1007/s00894-021-04800-6

65. M. Thirunavukkarasu, G. Balaji, S. Muthu, B.R. Raajaraman, and P. Ramesh, "Computational Spectroscopic Investigations on Structural Validation with IR and Raman Experimental Evidence, Projection of Ultraviolet-Visible Excitations, Natural Bond Orbital Interpretations, and Molecular Docking Studies under the Biological Investigation on N-benzyloxycarbonyl-L-Aspartic Acid 1-Benzyl Ester," *Chemical Data Collections* 31 (2021): 100622. https://doi.org/10.1016/j.cdc.2020.100622

66. G. Muteeb, A. Alsultan, M. Farhan, and M. AAtif, "Risedronate and Methotrexate Are High-Affinity Inhibitors of New Delhi Metallao-β-Lactamase-1 (NDM-1): A Drug Repurposing Approach," *Molecules* 27, no. 4 (2022): 1283. https://doi.org/10.3390/molecules27041283

67. J.S. Al-Otaibi, Y.S. Mary, S. Fazil, Y.S. Mary, and S. Sarala, "Modeling the Structure and Reactivity Landscapes of a Pyrazole-Ammonium Ionic Derivative Using Wavefunction-Dependent Characteristics and

Screening for Potential Anti-Inflammatory Activity," *Journal of Biomolecular Structure and Dynamics* (2021): 1–13. https://doi.org/10.1080/07391102.2021.1957020

68. Y.S. Mary, Y.S. Mary, S. Armakovic, S.J. Armakovic, R. Yadav, I. Celik, and R. Razavi, "Investigation of Reactive Properties, Adsorption on Fullerene, DFT, Molecular Dynamics Simulation of an Anthracene Derivative Targeting Dihydrofolate Reductase and Human dUTPase," *Journal of Biomolecular Structure and Dynamics* (2021): 1–10. https://doi.org/10.1080/07391102.2021.1953602

69. J.S. Al-Otaibi, Y.S. Mary, Y.S. Mary, and R. Yadav, "Structural and Reactivity Studies of Pravadoline – An Ionic Liquid, with Reference to Its Wavefunction-Relative Properties Using DFT and MD Simulations," *Journal of Molecular Structure* 1245 (2021): 131074. https://doi.org/10.1016/j.molstruc.2021.131074

70. Y.S. Mary, Y.S. Mary, A. Bielenica, S. Armakovic, S.J. Armakovic, V. Chandramohan, and M. Dammalli, "Inevstigation of the Reactivity Properties of a Thiourea Derivative with Anticancer Activity by DFT and MD Simulations," *Journal of Molecular Modeling* 27, no. 8 (2021): 217. https://doi.org/10.1007/s00894-021-04835-9